Pergamon

Chemical Engineering Science, Vol. 51, No. 20, pp. 4619–4629, 1996

0009-2509/96 $15.00 + 0.00

PII: S0009-2509(96)00265-5

SIZE, STRUCTURE AND DYNAMICS OF "LARGE" BUBBLES IN A TWO-DIMENSIONAL SLURRY BUBBLE COLUMN

J. W. A. DE SWART, R. E. VAN VLIET and R. KRISHNA*
Department of Chemical Engineering, University of Amsterdam, Nieuwe Achtergracht 166, 1018 WV Amsterdam, The Netherlands

(*First received* 16 *November* 1995; *revised manuscript received and accepted* 28 *February* 1996)

Abstract This paper reports preliminary results of a study on the hydrodynamics of a two-dimensional slurry bubble column. Experiments have been carried out with air paraffin oil slurries with solids concentrations of 0, 28.3 and 38.6 vol% of porous silica particles (mean diameter of 38 μm). Bubble sizes, bubble coalescence and bubble break-up rates were determined by video image analysis. Increasing slurry concentration increases the size and size distribution of the "large" bubbles, defined here as having diameters larger than 10 mm. Increasing slurry concentration reduces the total gas holdup to a significant extent; this reduction is to be largely attributed to the destruction of the "small" bubble population, which have bubble diameters smaller than 10 mm. Video imaging experiments lead to new insights into the mass transfer mechanisms from "large" bubbles. These "large" bubbles are continually coalescing and breaking up. The coalescence and breakup rates were determined by a frame-by-frame analysis of the video recordings and found to be at least 4 s^{-1}. A population model for mass transfer has been set up and used to establish that frequent bubble–bubble interactions could lead to an order of magnitude increase in the mass transfer rates for the large bubble class. Copyright © 1996 Elsevier Science Ltd

Keywords: Bubble columns, large bubbles, small bubbles, bubble size distribution, gas holdup, bubble coalescence, bubble breakup.

INTRODUCTION

The bubble column slurry reactor is an attractive reactor type for relatively slow, exothermic liquid phase catalytic processes. For example, for the industrially important Fischer Tropsch synthesis of hydrocarbons from synthesis, Fox (1990), Jager and Espinoza (1995) and De Swart *et al.* (1995) have concluded that the bubble column slurry reactor, operating in the churn-turbulent regime, is to be preferred to the multi-tubular trickle bed technology on both technical and economic grounds. In the churn-turbulent regime of operation of a bubble column, "large" and "small" bubbles are known to co-exist (Ellenberger and Krishna, 1994; Krishna and Ellenberger, 1995). The "large" bubbles, which have rise velocities typically of the order of 1.5 m s^{-1}, largely dictate the gas phase conversion in the churn-turbulent regime. Though the hydrodynamics of bubble columns slurry reactors has been studied by several workers [see e.g. Deckwer *et al.* (1980, 1992, 1993); Kara *et al.* (1982); Koide *et al.* (1984); Kelkar *et al.* (1984); Fukuma *et al.* (1987); Schumpe *et al.* (1987); O'Dowd *et al.* (1987); Bukur *et al.* (1987, 1990); Saxena *et al.* (1992, 1993, 1995); De Swart and Krishna (1995)], there is no study in which the characteristics of these "large" bubbles have been elucidated. The broad objective of the present study is to provide information on the size and structure of these "large" bubbles by use of video imaging techniques in a two-dimensional column. A frame-by-frame analysis of the video images also provided some fresh insights into the coalescence-breakup phenomenon of the "large" bubble population.

A further issue which has been addressed in this paper is the mass transfer from "large" bubbles. Vermeer and Krishna (1981) measured the volumetric mass transfer coefficients from the large bubbles in the system nitrogen–turpentine and found values about an order of magnitude higher than that expected on the basis of the visually observed bubble sizes for churn-turbulent operation. They attributed the measured high values of mass transfer coefficients to the violently turbulent nature of the liquid phase. In the present paper, we examine whether bubble–bubble interactions are the likely cause of the paradoxically high mass transfer coefficients; Sit and Grace (1981) have shown that bubble–bubble interactions in a gas–solid bubbling fluid bed leads to an improvement in the interphase mass transfer rate and one may wonder if an analogous phenomenon exists for gas–liquid (slurry) bubble columns.

EXPERIMENTAL SET UP AND SYSTEMS STUDIED

All experiments were carried out in a two-dimensional column consisting of two parallel 7 mm thick glass plates of 2.5 m height and 0.3 m width, placed at a distance of 0.005 m. The gas phase was distributed into the column by a glass sintered plate with a pore diameter of 200 μm. The column was equipped with

*Corresponding author. E-mail: krishna@chemeng.chem.uva.nl.

a quick closing valve placed near the gas distributor. A pressure tap was installed at 1.20 m height. The total gas holdup was determined from measurements of the static pressure drop using high accuracy Validyne DP15 pressure transducers. A Panasonic DSP colour CCD camera was placed perpendicular to the column at a distance of 1.15 m from the front face. The camera either recorded at a height of 0.65 or 1.15 m from the gas distributor plate. A shutter speed of 1/2000 was employed to avoid blurring of the video images due to the motion of the gas bubbles. To improve the contrast between the bubbles and the liquid phase, the technique of diffuse backlighting was used (Lunde and Perkins, 1995) and ppm quantities of dye Sudan green 988 were added to the liquid. Two 1250 W halogen lamps were directed on a white panel to provide a smooth and even background. The video signal produced by the camera was digitized at a rate of 25 frames per second using a Miro VIDEO DC1 digitizer board placed inside a PC. The real time signals were directed to a Sony colour video monitor for on-line control of the camera output. The captured images were transferred to a PC and processed using the commercial image processing software SCIL-Image™. SCIL-Image™ is developed by the Computer Systems Group of the University of Amsterdam and TNO Institute of Applied Physics in Delft, The Netherlands. Figure 1 shows the experimental setup schematically.

Paraffinic mineral oil (density, $\rho_L = 800\ kg\,m^{-3}$; viscosity, $\mu_L = 0.027\ Pa\,s$; surface tension, $\sigma = 0.028\ N\,m^{-1}$) was used as liquid phase. Air was used as the gas phase in all experiments and porous silica particles (skeleton density = $2100\ kg\,m^{-3}$; pore volume = $1.05\ ml\,g^{-1}$; particle size distribution: 10%, $< 27\ \mu m$; 50%, $< 38\ \mu m$; 90%, $< 47\ \mu m$) formed the suspended solids. Experiments were carried out with solids concentration of 0, 28.3, and 38.6 vol% solids (on a gas-free slurry basis).

IMAGE ANALYSIS

At a given superficial gas velocity U and height above the distributor h, one experimental run for image processing purposes is performed. An experimental run consists of three samples of eight seconds, resulting in 600 images. The captured images are of the Tagged Interchange File Format (TIFF) with 24 bit color depth and an aspect ratio of 1:1. After capturing, the images are separately processed using the SCIL-Image™ software package. Using this software package several image processing steps can be automated, which is a necessity when analyzing large amounts of data. The first step in the image processing is the conversion of the 24 bit (true color) images into 8 bit (gray scale) images. Each pixel in the image has now a so-called gray value ranging from 0 to 255. A gray value of 0 corresponds to black and a gray value of 255 to white. A region of interest is then defined by cropping the image to 260×276 pixels, representing the 0.3×0.3 m window of observation in the column. One pixel length is therefore approximately equal to 1 mm distance. A typical picture resulting from the first image processing steps is shown in Fig. 2 (a) for the air/paraffin oil system.

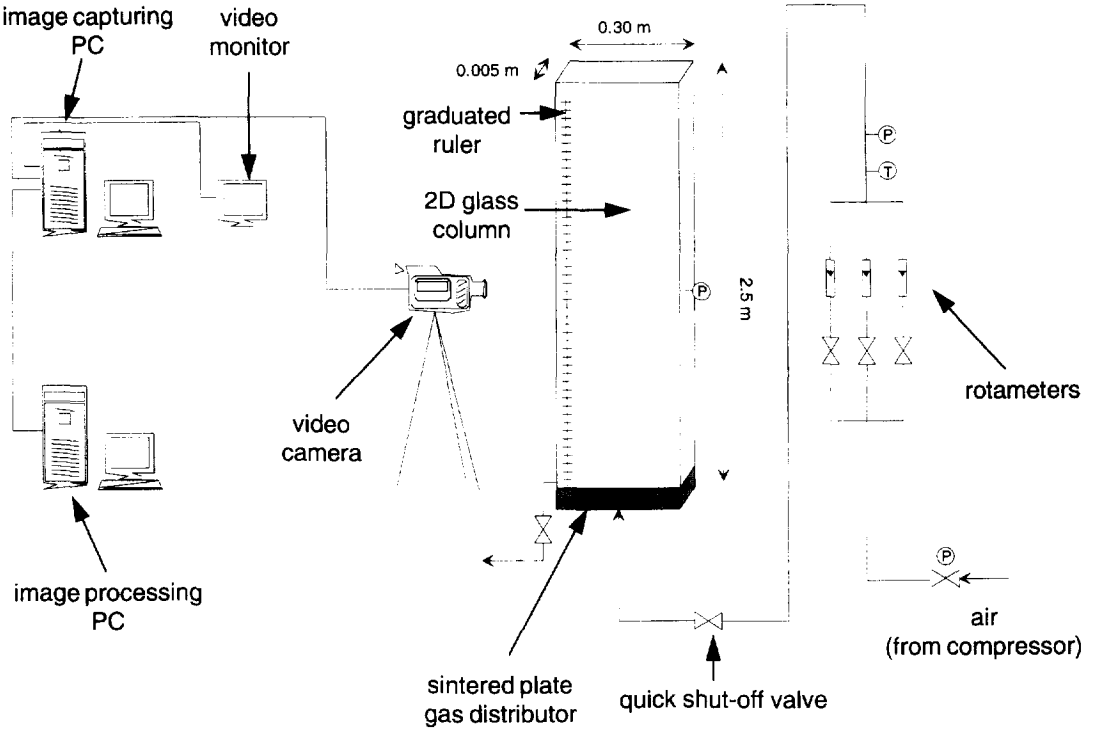

Fig. 1. Experimental setup for the two-dimensional column.

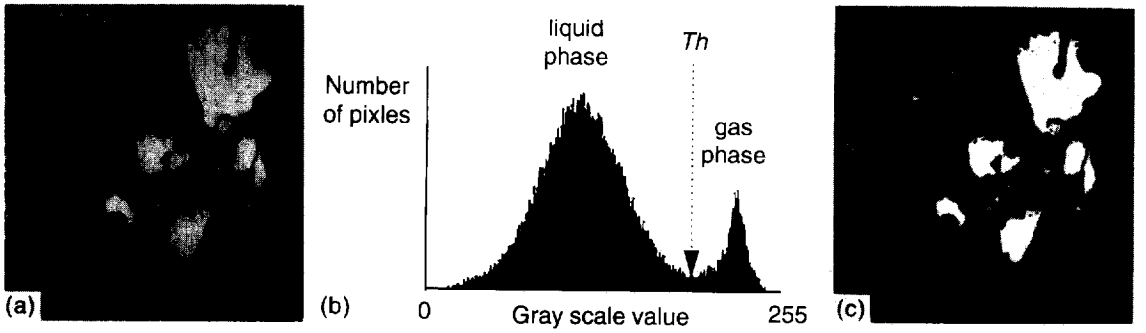

Fig. 2. (a) Image processing: gray value image; (b) gray value distribution of image; (c) binary image resulting after segmentation of the gray value image by thresholding.

The next step is the segmentation of the images. Segmentation is the process that subdivides an image into its constituent parts or objects (Gonzales and Wintz, 1987). The most common way to establish this is to apply the technique of thresholding. This can either be done by deciding a threshold level or by using the entropy method (Kapur *et al.*, 1985). Figure 2(b) shows the gray level distribution of the objects seen in Fig. 2(a). It can be seen that the gray level distribution is almost bimodal. Therefore, the optimal threshold gray value Th lies between the peaks of the distribution, as indicated in Fig. 2(b). For any given coordinate (x, y) in an image with a grey level $f(x, y)$, the thresholding operation can be expressed as:

$$g(x, y) = \begin{cases} 1 & \text{if } f(x, y) \geqslant \text{Th} \\ 0 & \text{if } f(x, y) < \text{Th} \end{cases}, \tag{1}$$

where $g(x, y)$ is the grey level of the corresponding picture in the resulting binary image.

Application of this thresholding to Fig. 2(a) results in the binary image shown in Fig. 2(c). The entropy method for thresholding an image is preferable when the two peaks in the gray level distribution are separated by a wide and flat valley. As this is not the case in the present experiment, the threshold level is chosen by visual inspection as indicated in Fig. 2(b); due to the sharp valley in the histogram there is no ambiguity regarding the value of Th. Note that no image enhancement has been applied in order to preserve as much of the "raw" data as possible. The binary image is then subdivided ("labelled") into different components, based upon a connectivity analysis. The last step in the analysis of the images is the measurement of the shape of each object in the image. Object properties such as area, perimeter, width and height can be measured. The present study is focused on the area of the objects.

After completion of the image analysis the data have to be processed. As the aspect ratio of the images is 1 : 1, the number of pixels that form an individual bubble are easily converted to the bubble area A_b by multiplying with a linear scale factor. The equivalent bubble diameter can be calculated directly from the bubble area:

$$d_b = \sqrt{\frac{4}{\pi} A_b}. \tag{2}$$

The calculation of the gas holdup in an image follows from:

$$\varepsilon = \frac{\sum A_{\text{obj}}}{A_{\text{im}}}. \tag{3}$$

where A_{obj} is the area of one object in pixels and A_{im} represents the total area of the image (i.e. $260 \times 276 = 71,760$ pixels). The same expression can also be used to calculate the gas holdup of a certain bubble size class; in this case A_{obj} represents the area occupied by one object in that bubble class. The procedure was first calibrated by video imaging objects (circles, squares) of known areas.

TOTAL GAS HOLDUP, BUBBLE SIZE AND BUBBLE SIZE DISTRIBUTION

Figure 3 shows the total gas holdup vs the superficial gas velocity for air/paraffin slurries containing 0, 28.3 and 38.6 vol% silica particles. The total gas holdup decreases significantly with increasing solids concentration. The same trend has been found for columns of circular cross section by Koide *et al.* (1984), Kara *et al.* (1982), Kelkar *et al.* (1984), De Swart and Krishna (1995) and Yasunishi *et al.* (1986).

The effect of the superficial gas velocity and the solids concentration on the bubble size distribution was investigated using image analysis. For each experimental run the bubble size distribution was calculated using 600 frames (corresponding to 24 s video recording). To show the gas holdup structure the bubble size distributions are expressed in individual gas fractions in the column. Figure 4 shows the influence of the superficial gas velocity on the bubble size distribution for paraffin oil. Increasing the superficial gas velocity leads to formation of larger bubbles and also increases the bubble size distribution. In Fig. 5 the bubble size distribution is shown for paraffin oil slurries of 0, 28.3 and 38.6 vol% concentration. For these three series the superficial gas velocity is kept

constant at a value of around 0.10 m s^{-1}. It can be seen that as the solids concentration is increased the "small" bubbles, smaller than say 10 mm in size, disappear, their contribution to the gas holdup decreases significantly. Furthermore, the bubble size distribution broadens and the average bubble size becomes larger. Figure 6 shows three grabbed, and retraced, video images as visual support for this conclusion; from these pictures it can clearly be seen that the "small" bubbles disappear and the "large" bubbles become larger as the solids concentration is increased.

Frame-by-frame visual examination of the video images also revealed that bubbles smaller than 10 mm have the backmixing characteristics of the liquid phase. Bubbles larger than 10 mm, on the other hand, traversed up the column virtually in plug flow. The "large" bubble population can therefore be defined as having bubble sizes larger then 10 mm. Using the SCIL-Image™ software all objects smaller than 10 mm can be automatically removed in order to focus on the "large" bubble population; see Figs 7(a) and (b). For the 28.3 and 38.6 vol% slurry concentrations, the bubble population smaller than 10 mm is virtually destroyed (*cf.* Fig. 6) and the whole bubble population can be considered to be "large".

The average "large" bubble size increases with increasing superficial gas velocity and slurry concentration; see Fig. 8. For the 28.3 vol% slurry concentrations, the average bubble size has been measured at heights $H = 0.65$ and 1.15 m above the distributor. The results show a slight increase in the average bubble diameter with increasing H, pointing to increasing coalescence as one proceeds up the column.

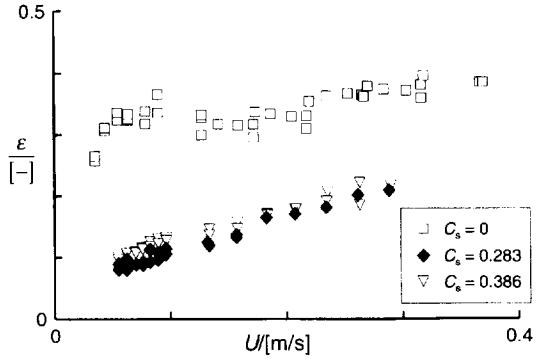

Fig. 3. Influence of increased solids concentration on the total gas holdup with air/paraffin slurries.

BUBBLE–BUBBLE INTERACTIONS

In order to gain further insights into the mechanism of mass transfer from the large bubble population we resorted to a careful frame-by-frame analysis of the video recordings. Figure 9 shows eight sequential pictures (frames) taken from an experimental run with the 28.3 vol% paraffin oil slurry at a superficial gas velocity of 0.09 m s^{-1}. The time interval between the individual frames is 40 ms and the "small" bubbles, smaller than 10 mm, have been filtered out. Two bubbles A and B are followed as they rise through the column. It can be seen from frames 1 to 4 that bubble B rises faster than bubble A. In frame 5 bubble

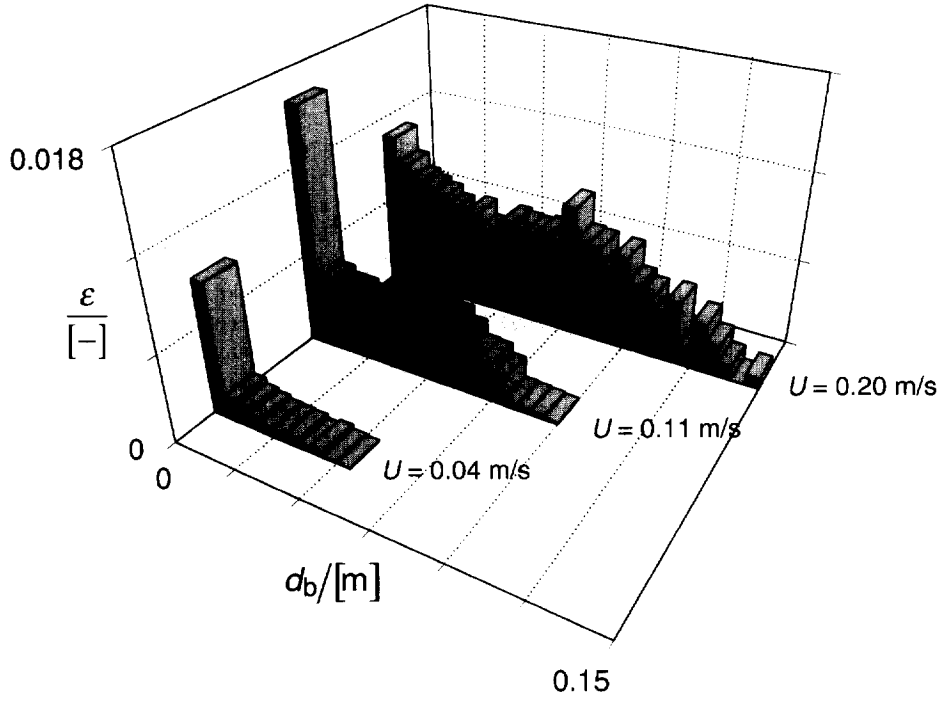

Fig. 4. Influence of the superficial gas velocity on the gas holdup structure for the system: air/paraffin oil. Measurements made at a height $H = 0.65$ m above the distributor.

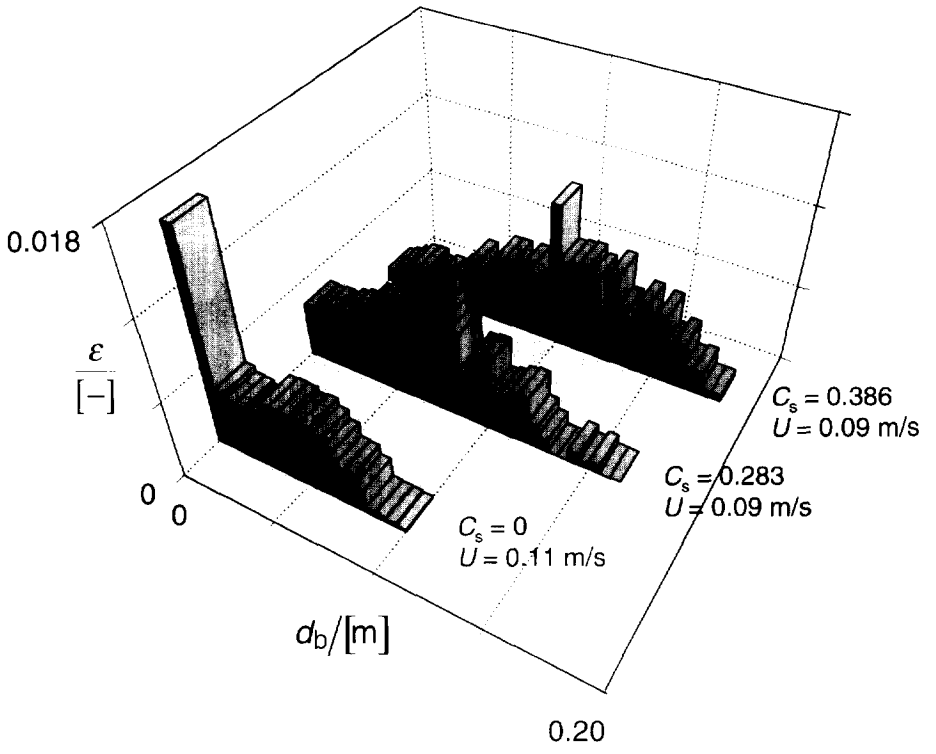

Fig. 5. Influence of increased solids concentration on the gas holdup structure for the system air/paraffin oil slurries. Measurements made at a height $H = 0.65$ m above the distributor.

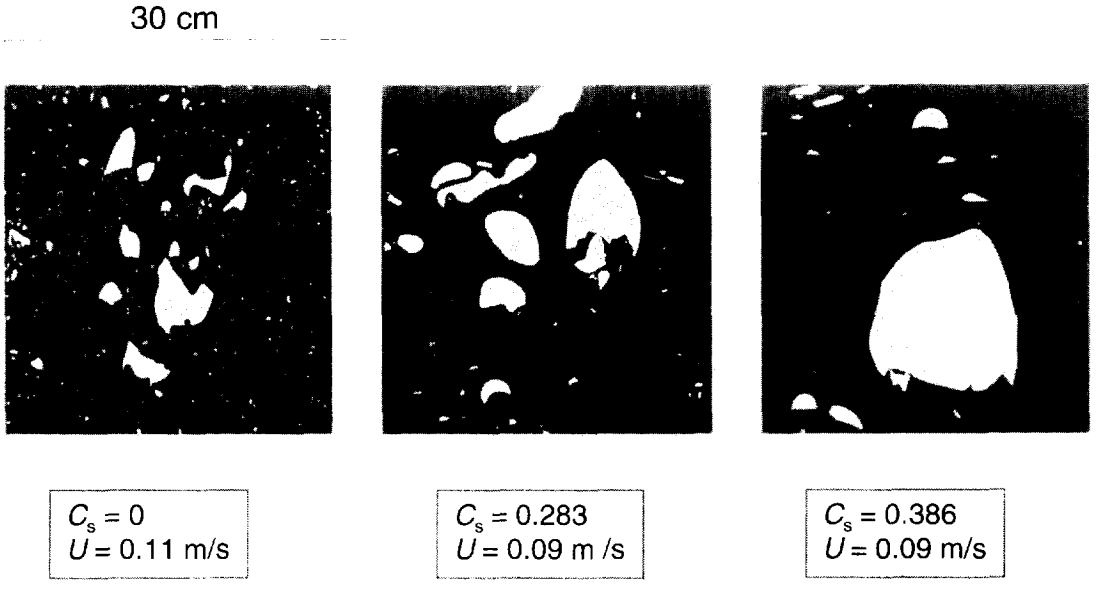

Fig. 6. Influence of increased particle concentration: impression of three retraced video images obtained at 0.65 m above the distributor.

B reaches the wake of bubble A and coalescence follows; in frame 6, A and B are coalesced and bubble AB is formed. Bubbles D and E in frame 7 coalesce to form DE in frame 8. Let us now track the history of bubble C in frames 1, 2, 3 and 4. In frame 4 bubble C breaks up into bubbles C1 and C2.

To obtain quantitative data on the bubble break-up and coalescence rates for the 28.3 vol% slurry at

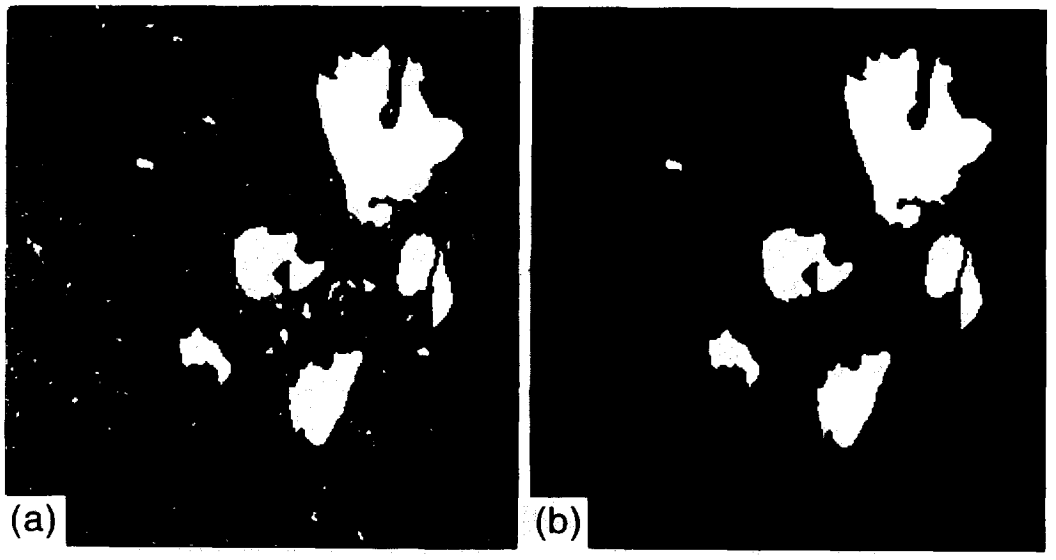

Fig. 7. Image processing: filling of "gaps" in the binary image (b) removal of objects smaller than 10 mm from the image.

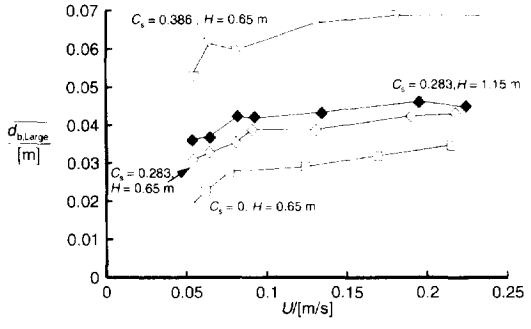

Fig. 8. Influence of superficial gas velocity and slurry concentration on the mean diameter of the "large" bubble population. Measurements at $H = 0.65$ m above the distributor for air/paraffin oil slurries for 0, 28.3 and 38.6 vol% slurries and at $H = 1.15$ m for the 28.3 vol% slurry.

a superficial gas velocity of 0.09 m s^{-1}, a detailed frame-by-frame analysis of the 8-s recording, equivalent to 200 frames, was carried out. Firstly, the "large" bubble population, defined as indicated above by using a cut-off bubble size of 10 mm, was split up in 6 different bubble size classes (0.01–0.02, 0.02–0.04, 0.04–0.06, 0.06–0.08, 0.08–0.1 and > 0.1 m). For each of these bubble classes, individual bubbles were visually tracked to determine the death rates, defined as the fraction of the gas holdup in the bubble class under consideration which disappears by either coalescence or break-up to other bubble size classes. A parallel analysis was carried out to determine the birth rate of a certain bubble class, representing the creation of the gas fraction per second by a process of coalescence or breakup of other bubble size classes. By a class-by-class analysis of 200 consecutive frames, the birth and death rates were calculated; these are shown in Fig. 10. It is to be noted that for each bubble class the birth and death rates are close to each other, as would be expected for a system at dynamic equilibrium in which the bubble size distribution is preserved. Let us denote s_{Bi} as the refreshment rate, birth or death rate, of the bubble class i, with the units s^{-1}. We note that that s_{Bi} increases as the size of the bubble class increases. Put another way, larger sized bubbles are refreshed more often, due to coalescence and break-up than smaller sized bubbles; this is in conformity with our intuition. The refreshment frequency for the smallest size class 1 (with an average diameter of 0.015 m) is about 4 s^{-1}. The refreshment frequency increases to about 15 s^{-1} for largest bubble size class 6 (diameters larger than 0.1 m). Larger sized bubble classes therefore "suffer" more frequent interchange with other bubble classes.

Further, some idea of interchange between bubble classes was obtained by tracking the number of bubbles in class i which break-up or coalesce into class j. The bubble exchange matrix for the 28.3 vol% slurry is shown in Table 1. This shows that the number of bubbles involved in the bubble class interchange process decreases with increasing bubble size class. If a sufficiently large number of frames is analyzed, the bubble exchange matrix might be expected to be symmetric; our results in Table 1 show this matrix to be nearly symmetric.

Summarizing in words the findings of Fig. 10 and Table 1, we can say that larger bubble size classes are refreshed more frequently but a smaller number of these are involved in an interchange process. The bubble–bubble exchange rate between any two classes can be expected to be dictated by the refreshment rate of the smaller bubble class s_{Bi}. For example, interchange between classes 1 and 2 can be expected to be at a frequency of, say, 4 s^{-1}.

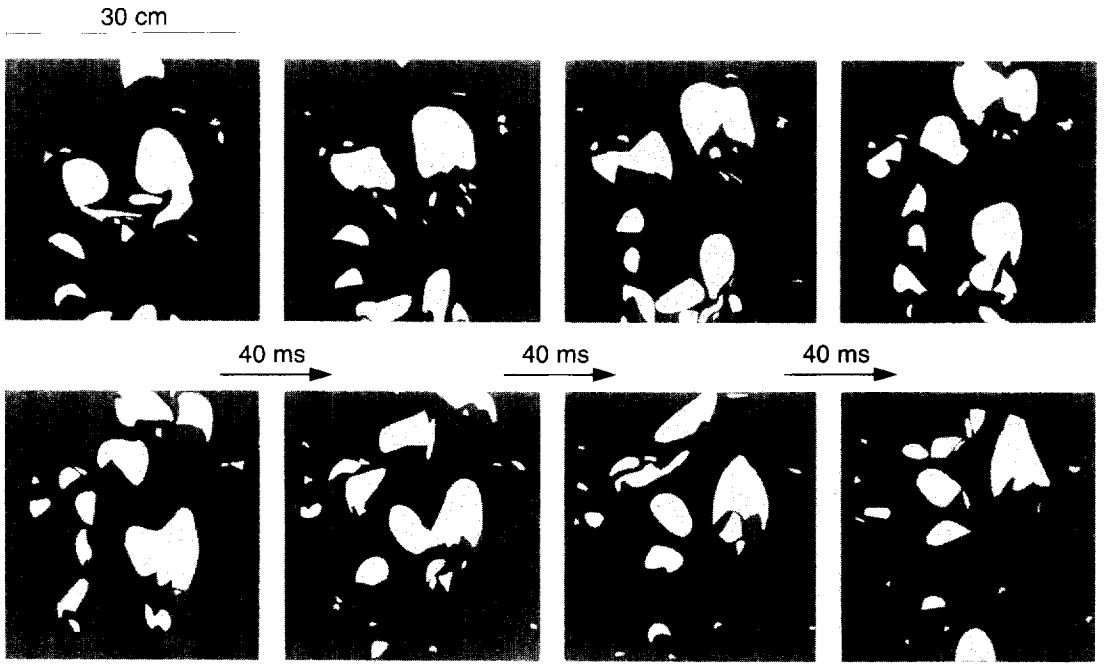

Fig. 9. Eight consecutive frames of the air/28.3 vol% oil slurry: coalescence of the large bubbles. Recorded at a height of 0.65 m and a superficial gas velocity of 0.09 m s^{-1}.

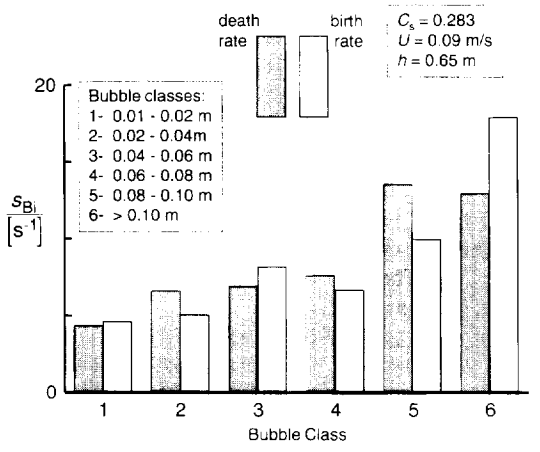

Fig. 10. Birth and death rates for different bubble classes, expressed as the fraction of the gas holdup of a bubble class which is lost (death) or gained (birth) due, respectively to breakup or coalescence. System: air 28.3 vol% oil slurry, recorded at a height of 0.65 m and a superficial gas velocity of 0.09 m s^{-1}.

Table 1. Bubble exchange matrix

From to	Class 1	Class 2	Class 3	Class 4	Class 5	Class 6
Class 1	×	31	16	5	9	4
Class 2	43	×	30	10	8	10
Class 3	12	22	×	10	4	8
Class 4	5	9	14	×	2	4
Class 5	6	7	5	5	×	3
Class 6	3	7	1	0	0	×

Note: The numbers represent the number of bubbles in a certain size class which undergo exchange with a different size class. The numbers were measured frame-by-frame for an eight second period over 200 frames of operation at superficial gas velocity of 0.09 m s^{-1} and slurry concentration of 28.3 vol%.

A POPULATION BALANCE MODEL FOR MASS TRANSFER FROM "LARGE" BUBBLES

For the "large" bubble population containing n bubble size classes, we envisage a mass transfer mechanism as pictured in Fig. 11. Each bubble class exchanges mass with the liquid (or slurry) phase with a transfer coefficient $k_{L,i}a_i$. Further, to account for the bubble–bubble interactions we assume that each bubble class exchanges mass with every other bubble class, either by a process of coalescence or break-up, with an exchange coefficient E_{ij}, expressed in the units s^{-1}.

For each bubble class, we define the number of mass transfer units for transfer to the liquid phase

$$\mathrm{NTU}_i = \frac{k_{L,i}a_i H}{U_{\mathrm{Large},i}}, \tag{4}$$

where $U_{\mathrm{Large},i}$ is the superficial gas velocity through the "large" bubble population i. The number of exchange transfer units for direct exchange of mass between classes i and j

$$\mathrm{NExTU}_{ij} = \frac{E_{ij}\varepsilon_i H}{U_{\mathrm{Large},i}}, \tag{5}$$

where E_{ij} is the exchange coefficient between the bubble classes i and j. Exchange of gas between the bubble classes does not alter their gas holdups; this

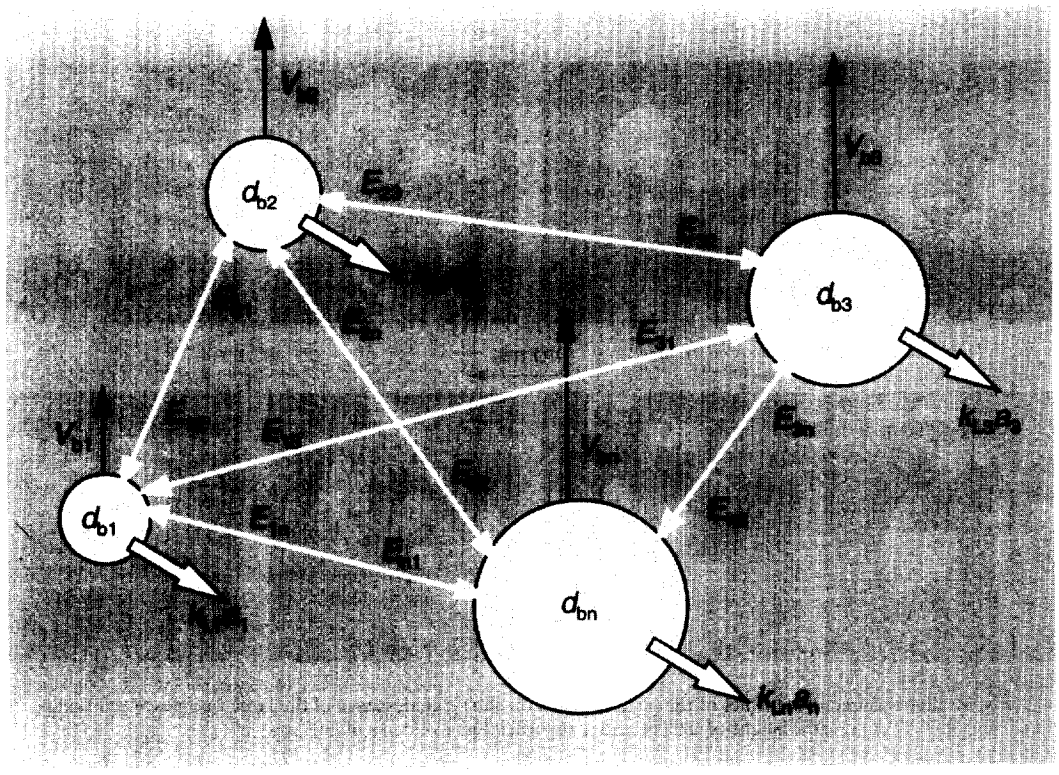

Fig. 11. Mass transfer model for transfer from "large" bubbles involving bubble–bubble interchange coefficients E_{ij} and transfer coefficients to the liquid phase $k_{L,i}a_i$.

implies that we have the relation

$$E_{ij}\varepsilon_i = E_{ji}\varepsilon_j. \tag{6}$$

The bubble refreshment rate s_{Bi} of class i is then:

$$s_{Bi} = \sum_{j=1, j\neq 1}^{n} E_{ij} \tag{7}$$

$$\frac{d(C_g)}{d\xi} = [A](C_g) + (B)C_L, \tag{8}$$

where ξ is the dimensional distance along the reactor ($\xi \equiv h/H$). (C_g) is the n-dimensional column matrix of gas phase concentrations in the individual bubble classes, C_{gi}. The $n \times n$ dimensional transfer coefficient matrix [A] has the elements

$$[A] = \begin{bmatrix} -\dfrac{\mathrm{NTU}_1}{m} - \sum\limits_{\substack{j=1\\ j\neq 1}}^{n} \mathrm{NExTU}_{1j} & \mathrm{NExTU}_{12} & \cdots & \mathrm{NExTU}_{1n} \\ \mathrm{NExTU}_{21} & -\dfrac{\mathrm{NTU}_2}{m} - \sum\limits_{\substack{j=1\\ j\neq 2}}^{n} \mathrm{NExTU}_{2j} & \cdots & \mathrm{NExTU}_{2n} \\ \vdots & \cdots & \ddots & \cdots \\ \mathrm{NExTU}_{n1} & \mathrm{NExTU}_{n2} & \cdots & -\dfrac{\mathrm{NTU}_n}{m} - \sum\limits_{\substack{j=1\\ j\neq n}}^{n} \mathrm{NExTU}_{nj} \end{bmatrix}, \tag{9}$$

The experimental results on the refreshment rates s_{Bi} (*cf.* Fig. 10) can then be used in conjunction with eqs (6) and (7) to estimate the values of the exchange coefficients E_{ij}.

Assuming plug flow of all the bubble classes, the differential equations for mass transfer to a completely mixed liquid phase, of uniform concentration C_L can be expressed in n-dimensional matrix notation as

where m is the distribution coefficient between gas and liquid phases.

The n-dimensional column matrix (B) has the elements

$$(B) = \begin{pmatrix} \mathrm{NTU}_1 \\ \mathrm{NTU}_2 \\ \vdots \\ \mathrm{NTU}_n \end{pmatrix}. \tag{10}$$

To demonstrate the influence of the exchange of gas between the classes on the overall mass transfer rate the model of n large bubble classes is now worked out in detail for three classes: class 1 with a bubble diameter $d_{b,1}$ of 0.01 m, class 2 with a bubble diameter $d_{b,2}$ of 0.04 m and class 3 with a bubble diameter $d_{b,3}$ of 0.1 m. The rise velocity of the 0.1 m bubbles is estimated from our experiments and equals 0.95 m s^{-1}. The bubble rise velocity is assumed to be proportional to d_b and so the rise velocity of the 0.01 m and 0.04 m diameter bubbles can now be calculated to be 0.3 m s^{-1} and 0.6 m s^{-1}, respectively. Mass transfer coefficients for each of the bubble classes are estimated from the surface renewal theory:

$$k_{L,i} = 2\sqrt{\frac{D}{\pi t_{c,i}}}, \tag{11}$$

where D is the diffusivity and t_c is the contact time between gas and liquid. The contact time is estimated from $t_{c,i} = d_{b,i}/V_{b,i}$ for each bubble class. The gas holdups of the three classes are estimated from the measured gas holdup structures ($\varepsilon_1 = 0.05$, $\varepsilon_2 = 0.06$, $\varepsilon_3 = 0.03$). The interfacial areas are calculated from $a = 6\varepsilon/d_b$; this yields $a_1 = 30$, $a_2 = 9$ and $a_3 = 1.8$ m^2 m^{-3}. The superficial gas velocities through each bubble class is $V_b\varepsilon$; this yields $U_{\text{Large},1} = 0.015$, $U_{\text{Large},2} = 0.036$ and $U_{\text{Large},3} = 0.028$ m s^{-1}.

Simulations are now carried out for conditions relevant for the Fischer–Tropsch synthesis. Hydrogen absorption from synthesis gas into paraffin oil at a pressure of 40 bar and a temperature of 513 K is considered. Hydrogen and carbon monoxide are present in the syngas feed at a ratio of 2. The superficial gas velocity through the total large bubble population, $U_{\text{Large}} = 0.079$ m s^{-1}, is assumed to be constant over the reactor height $H = 30$ m. The diffusivity D and distribution coefficient m of hydrogen are equal to 5.5×10^{-8} m^2 s^{-1} and 5, respectively. The concentration of hydrogen in the liquid phase is set at $C_L = 40$ mol m^{-3} and is assumed to be constant along the height of the reactor. From the data given in Fig. 10 and Table 1, and keeping in mind the constraints given by eqs (6) and (7), we have made rough estimates of the values of the exchange coefficients E_{ij} for the three-bubble classes: $E_{12} = 3$, $E_{13} = 1$, $E_{21} = 2.5$, $E_{23} = 3$, $E_{31} = 1.7$ and $E_{32} = 6$ s^{-1}. The refreshment rates calculated using eq. (7) for the three bubble classes are: $s_{B1} = 4$, $s_{B2} = 6.5$ and $s_{B2} = 7.7$ s^{-1}, which agrees with the trend portrayed in Fig. 10. The values of the numbers of mass transfer units are calculated from eqs (4) and (11) to be $\text{NTU}_1 = 83$, $\text{NTU}_2 = 7.3$ and $\text{NTU}_3 = 1.47$. The coefficient matrix [A] can now be calculated from eq. (9) and the set of ordinary linear differential equations (8) can be solved to yield the composition profiles for hydrogen in the gas phase along the height of the reactor. Figure 12 shows the dimensionless hydrogen concentration ($C_{g,H2}/C_{g0,H2}$) profile along the column height. The three profiles coincide with one another

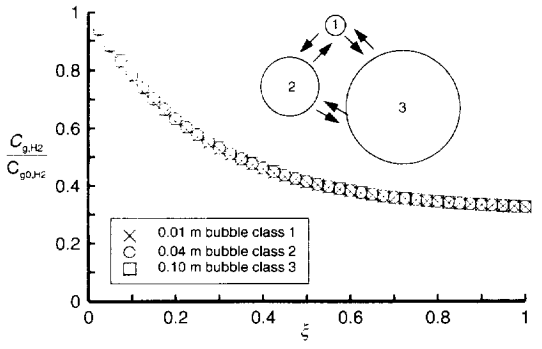

Fig. 12. Relative hydrogen concentration as a function of axial position in a Fischer Tropsch slurry reactor operating at a superficial gas velocity of 0.079 m s^{-1}. Model calculations based on a three bubble class and interaction coefficients as shown in the figure. The continuous line corresponds to the ensemble average concentration calculated from eq. (12).

and the conversion at the reactor outlet is 68%. The conversion behaviour of the three bubble class system, with 0.01, 0.04 and 0.1 m diameter bubbles is found to be equivalent to that of a single bubble class system of diameter 0.021 m moving through the reactor at a superficial gas velocity $U = U_{\text{Large},1} + U_{\text{Large},2} + U_{\text{Large},3} = 0.079$ m s^{-1}. Put another way, due to frequent bubble–bubble interchange, the effective bubble diameters for the 0.04 and 0.1 m diameter classes are reduced to about 0.02. This implies an enhancement for the 0.1 m bubble class of five.

In order to further demonstrate the significance of the bubble–bubble interchange, we also carried our simulations taking all the exchange coefficients E_{ij} to be zero. The gas phase concentration profiles for the three bubble classes in this case are shown in Fig. 13. The 0.01 m bubble class equilibrates with the liquid phase very quickly whereas we see that the conversion obtained from the 0.1 m bubble class is extremely limited. Also shown in Fig. 13 is the weighted average concentration profile of the bubble ensemble calculated from:

$$\frac{dC_g}{d\xi} = \sum_{i=1}^{n} \frac{U_{\text{Large},i}}{U} C_{g,i}. \tag{12}$$

The overall conversion achieved by the ensemble is only 43%, significantly lower than that obtained taking interactions into account.

A further point to note is that the refreshment frequencies due to coalescence or break-up are of the same order of magnitude as the Danckwerts surface renewal frequencies for mass transfer. For a bubble of 0.1 m diameter the Danckwerts surface renewal frequency is calculated to be of the order of 3 s^{-1} while we see from Fig. 10 that this bubble class is refreshed at the rate of 15 s^{-1}. This implies that during the time span of unsteady-state transfer to the liquid phase, a bubble would lose its identity, resulting in a further

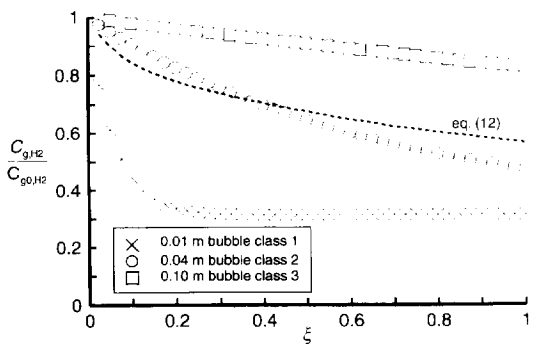

Fig. 13. Relative hydrogen concentration as a function of axial position in a Fischer Tropsch slurry reactor for the three bubble class without bubble–bubble interchange. Also shown in dashed lines are calculations of the ensemble averaged concentrations along the reactor height following eq. (12).

enhancement of the mass transfer coefficient k_L, estimated to be of the order of a factor 2. A detailed mass transfer model needs to be set up to take this also into account. A combination of bubble–bubble interchange and enhanced k_L due to accelerated surface renewal leads to an order of magnitude increase in the mass transfer coefficient above that estimated from "conventional" treatments ignoring bubble–bubble interactions.

Vermeer and Krishna (1981) in a study of mass transfer from "large" bubbles with the system air/turpentine had attributed the measured (paradoxically) high values of mass transfer coefficients to the violently turbulent nature of the liquid phase. We can now establish, albeit qualitatively, that frequent bubble–bubble exchanges are the most likely cause of high mass transfer rates.

CONCLUSIONS

We have gained some insight into the hydrodynamics of slurry bubble columns. Increasing slurry concentration reduces the total gas holdup; this reduction is to be largely attributed to the destruction of the "small" bubble population, which have bubble diameters smaller than 10 mm. Increasing slurry concentration increases the size and size distribution of the "large" bubbles. A frame-by-frame analysis of the video images shows that there is frequent bubble coalescence and breakup. With the aid of a population model for mass transfer we have established that this could lead to an order of magnitude increase in the mass transfer for the larger bubble sizes.

In view of the demonstrated significance of bubble–bubble interactions in a two-dimensional column, we consider it vital to confirm this phenomenon in a three-dimensional column with the aid of say tomographic techniques or fibre optic probes. A recent study, using video imaging techniques, by Stewart (1995) of bubble interactions in a three-dimensional column of 0.2×0.2 m cross section indicates coalescence-breakup rates of the order of 10–30 s^{-1}, providing some confirmation of our two-dimensional results.

Another aspect which deserves further study is the influence of the particle size and shape on the bubble hydrodynamics; in a recent study by Tsuchiya and Furumoto (1995) the influence of particle shape has been emphasised.

NOTATION

a	interfacial area per unit volume of dispersion, $m^2\ m^{-3}$
A	transfer coefficient matrix defined by eq. (7)
A_b	bubble area, m^2
A_{im}	total area of the image, pixels
A_{obj}	area of one object in an image, pixels
B	column matrix defined by eq. (8)
C_g	gas phase concentration, mol m^{-3}
C_{g0}	gas phase concentration at inlet to reactor, mol m^{-3}
C_L	liquid phase concentration, mol m^{-3}
C_s	solids volume fraction in gas free slurry
d_b	bubble diameter of the large bubble population, m
$d_{b,Large}$	mean bubble diameter of dilute phase, m
D	liquid phase diffusivity, $m^2\ s^{-1}$
E_{ij}	exchange coefficient of bubble class i with bubble class j, s^{-1}
h	height above the gas distributor, m
H	height of expanded bed, m
k_L	liquid phase mass transfer coefficient, s^{-1}
m	distribution coefficient
NTU	number of transfer units
NExTU	number of exchange transfer units
s_B	refreshment rate (birth or death rate), s^{-1}
t_c	contact time, s
Th	threshold grayscale value
U	superficial gas velocity, m s^{-1}
$U_{Large,i}$	superficial velocity of gas through the large bubble population i, m s^{-1}
U_{df}	superficial velocity of gas through the small bubbles, m s^{-1}
V_b	rise velocity of the large bubble population, m s^{-1}

Greek letters

ε	gas voidage
μ_L	liquid viscosity, Pa s
ρ_L	liquid density, kg m^{-3}
σ	surface tension of liquid phase, N m^{-1}
ξ	axial coordinate, h/H

Subscripts

g	referring to gas phase
$H2$	hydrogen
i	ith bubble class
L	referring to liquid phase
Large	referring to the large bubble population
0	referring to entrance to reactor
1,2,3	referring to bubble classes

REFERENCES

Bukur, D. B., Patel, S. A. and Matheo, R., 1987. Hydrodynamic studies in Fischer–Tropsch derived waxes in a bubble column. *Chem. Engng Commun.* **60**, 63–78.

Bukur, D. B., Patel, S. A. and Daly, J. G., 1990. Gas holdup and solids dispersion in a three phase slurry bubble column. *A.I.Ch.E. J.* **36**, 1731–1735.

Deckwer, W.-D., 1992. *Bubble Column Reactors*. Wiley, New York.

Deckwer, W.-D., Louisi, Y., Zaidi, A. and Ralek, M., 1980. Hydrodynamic properties of the Fischer–Tropsch slurry process. *Ind. Engng Chem. Process Des. Dev.* **19**, 699–708.

Deckwer, W.-D. and Schumpe, A., 1993. Improved tools for bubble column reactor design and scale-up. *Chem. Engng Sci.* **48**, 889–911.

De Swart, J. W. A. and Krishna, R., 1995. Effect of particles concentration on the hydrodynamics of bubble column slurry reactors. *Chem. Engng Res. Des., Trans. Instn Chem. Engng* **73**, 308–313.

De Swart, J. W. A., Krishna, R. and Sie, S. T., 1995. Selection, design and scale up of the Fischer–Tropsch reactor. *Studies in Surface Science and Catalysis*. Elsevier, Amsterdam, in press.

Ellenberger, J. and Krishna, R., 1994. A Unified approach to the scaleup of gas–solid fluidized and gas liquid bubble column reactors. *Chem. Engng Sci.* **49**, 5391–5411.

Fox, J. M., 1990. Fischer–Tropsch reactor selection. *Catal. Lett.* **7**, 281–292.

Fukuma, M., Muroyama, K. and Yasunishi, A., 1987. Properties of bubble swarm in a slurry bubble column. *J. Chem. Engng Japan* **20**, 28–33.

Gonzales, R. C., and Wintz, P., 1987. *Digital Image Processing*, 2nd Edition. Addison–Wesley Publishing Company, Ontario, Canada.

Jager, B. and Espinoza, R., 1995. Advances in low temperature Fischer–Tropsch synthesis. *Catal. Today* **23**, 17–28.

Kapur, J. N., Sahoo, P. K. and Wong, A. K. C., 1985. A new method for gray-level picture thresholding using the entropy of the histogram. *Comput. Graphics Image Process.* **29**, 273–285.

Kara, S., Kelkar, B. G., Shah, Y. T. and Carr, N. L., 1982. Hydrodynamics and axial mixing in a three-phase bubble column. *Ind. Engng Chem. Process Des. Dev.* **21**, 584–594.

Kelkar, B. G., Shah, Y. T. and Carr, N. L., 1984. Hydrodynamics and axial mixing in a three-phase bubble column. Effects of slurry properties. *Ind. Engng Chem. Process Des. Dev.* **23**, 308–313.

Koide, K., Takazawa, A., Komura, M. and Matsunaga, H., 1984. Gas hold-up and volumetric liquid-phase mass transfer coefficient in solid-suspended bubble columns. *J. Chem. Engng Japan*, **17**, 459–466.

Krishna, R. and Ellenberger, J., 1995. A unified approach to the scale up of "fluidized" multiphase reactors. *Chem. Engng Res. Des., Trans. Instn Chem. Engng* **73**, 217–221.

Lunde, K. and Perkins, R. J., 1995. A method for the detailed study of bubble motion and deformation. *Proc. 2nd Int. Conf. on Multiphase Flow*, '95 – Kyoto, Japan, pp. AV17–AV24.

O'Dowd, W., Smith, D. N., Ruether, J. A. and Saxena, S. C., 1987. Gas and solids behaviour in a baffled and unbaffled slurry bubble column. *A.I.Ch.E. J.* **33**, 1959–1970.

Saxena, S., 1995. Bubble column reactors and Fischer Tropsch synthesis. *Catal. Rev. Sci. Eng.* **37**, 227–309.

Saxena, S. C. and Rao, N. S., 1993. Estimation of gas holdup in slurry bubble with internals: nitrogen–therminol–magnetite system. *Powder Technol.* **75**, 153–158.

Saxena, S. C., Rao, N. S. and Thimmapuram, P. R., 1992, Gas phase holdup in slurry bubble columns for two- and three-phase systems. *Chem. Engng J.* **49**, 151–159.

Schumpe, A., Saxena, A. K. and Fang, L. K., 1987, Gas liquid mass transfer in a slurry bubble column. *Chem. Engng Sci.* **42**, 1787–1796.

Sit, S. P. and Grace, J. R., 1981. Effect of bubble interaction on interphase mass transfer in gas fluidized beds. *Chem. Engng Sci.* **36**, 327–335.

Stewart, C. W., 1995. Bubble interaction in low-viscosity liquids. *Int. J. Multiphase Flow* **21**, 1037–1046.

Tsuchiya, K. and Furumoto, A., 1995, Tortuosity of bubble rise path in a liquid–solid fluidized bed: effect of particle shape. *A.I.Ch.E. J.* **41**, 1368–1374.

Vermeer, D. J. and Krishna, R., 1981. Hydrodynamics and mass transfer in bubble columns operating in the churn-turbulent regime. *Ind. Engng Chem. Process Des. Dev.* **20**, 475–482.

Yasunishi, A., Fukuma, M. and Muroyama, K., 1986, Measurement of behaviour of gas bubbles and gas holdup in a slurry bubble column by a dual electroresistivity probe. *J. Chem. Engng Japan* **19**, 444–449.